

The Ultraviolet Radiation Environment of a Tropical Megacity in Transition: Mexico City

2000-2019

Adriana Ipiña,^{*,†,‡} Gamaliel López-Padilla,[¶] Armando Retama,[§] Rubén D. Piacentini,[†] and Sasha Madronich^{||}

[†]*Instituto de Física Rosario (CONICET-UNR), Rosario, Argentina*

[‡]*Centro de Ciencias de la Atmósfera, Universidad Nacional Autónoma de México, Mexico City, Mexico*

[¶]*Facultad de Ciencias Físico Matemáticas, Universidad Autónoma de Nuevo León, San Nicolás de los Garza, México*

[§]*Independent researcher, Mexico City, Mexico*

^{||}*National Center for Atmospheric Research, Boulder, Colorado, USA*

E-mail: ipina@ifir-conicet.gov.ar

Abstract

Tropical regions experience naturally high levels of UV radiation, but urban pollution can reduce these levels substantially. We analyzed 20 years of measurements of the UV Index (UVI) at several ground-level locations in the Mexico City Metropolitan Area and compared these data with UVI values derived from satellite observations of ozone and clouds (but not local pollution). The ground-based measurements were systematically lower than the satellite-based estimates, by ca. 40% in 2000 and 20% in 2019. Calculations with a radiative transfer model and observed concentrations of

9 air pollutants explained well the difference between satellite- and ground-based UVI,
10 and showed specific contributions from aerosols in the boundary layer and the free tro-
11 posphere, O₃, NO₂, and SO₂, in decreasing order of importance. Such large changes
12 in UV radiation between 2000 and 2019 have important implications ranging from hu-
13 man health (skin cancer and cataract induction) to air pollution control (photochemical
14 smog formation).

15 Introduction

16 Ultraviolet (UV) radiation is an important component of the urban environment, affecting
17 human populations directly through UV exposure of skin and eyes^{1–3} and less directly (but
18 with great impact) by driving the formation of photochemical smog, including tropospheric
19 ozone and other oxidants, as well as secondary aerosols containing nitrates, sulfates, and
20 organics.^{4–6} These pollutants, along with others of primary origin commonly found in ur-
21 ban atmospheres (e.g., black carbon, sulfur dioxide), can in turn scatter and/or absorb UV
22 radiation, alter its vertical distribution, and so modify the photochemical rate of their own
23 formation. Such feedback complicates the calculation of both the UV radiation field (in-
24 cluding at the surface), and the evolution of photochemical smog in the urban boundary
25 layer.

26 The question of how air pollution alters the urban UV environment (and *vice versa*) is
27 not new, but studies have relied mostly on numerical models,^{7–9} with relatively few available
28 observations (e.g., McKenzie et al.¹⁰, Panicker et al.¹¹, Palancar et al.¹², reviewed by Bais
29 et al.¹³). Increases in UV have been estimated as a consequence of emission reductions
30 over the last decades, e.g. in China,^{14–16} and have led to less-than-expected reductions in
31 photochemical smog, in part due to stronger UV photochemistry.^{17? ,18} Emission reductions
32 have also occurred globally during the 2020 COVID-19 pandemic,^{19,20} but ground-level ozone
33 in some polluted areas has actually increased,^{21,22} due at least in part to the increased UV
34 radiation. Unfortunately, the observational data base of relevant UV radiation remains

35 rather sparse to evaluate such model-derived hypotheses.

36 The environment of Mexico City is of particular interest for several reasons: (1) Nearly
37 23 million people inhabit the Mexico City Metropolitan Area (MCMA), and the UV en-
38 vironment has direct implications for their health, both in terms of skin/eye UV exposure
39 and *via* photochemical smog formation. (2) As a tropical megacity, it is to some extent
40 representative of the situation of many others, with year-round intense midday UV irradia-
41 nce, a shallower atmosphere due to the city's high elevation of 2240 m above sea level,
42 and a transition toward newer and cleaner technologies, leading to gradual improvements
43 in air quality. (3) Air quality within MCMA has undergone extensive scrutiny, with a well-
44 established monitoring network operating since 1986,²³ numerous intensive field campaigns
45 to study the meteorology, emissions, and photochemistry of smog formation,^{24–26} and numer-
46 ical modeling incorporating the evolving knowledge.^{27–30} This extensive body of knowledge
47 provides the foundation for understanding our study.

48 Here, we analyze two decades of continuous measurements of the UV Index at multiple
49 locations within the MCMA, collected by the Secretariat of the Environment (Secretaría
50 del Medio Ambiente, SEDEMA)¹ of the Mexico City government as part of an intensive
51 monitoring network over the MCMA. The UV Index is defined as:

$$UVI = 40 \int_{250nm}^{400nm} E(\lambda, t) \cdot S_{er}(\lambda) d\lambda \quad (1)$$

52 where $E(\lambda, t)$ is the solar spectral irradiance in units of $\text{W} \cdot \text{m}^{-2} \cdot \text{nm}^{-1}$ and $S_{er}(\lambda)$ is
53 the erythemal sensitivity of human skin.^{31,32} Multiplication by 40 was chosen historically to
54 express the UVI in small integer numbers, but is otherwise scientifically arbitrary.

55 The UVI is recognized by the World Health and Meteorological Organizations (WHO
56 and WMO) as a standardized metric of UV radiation³¹ for global public information. An
57 advantage of using the UVI as (one) measure of UV radiation is that it is being increasingly
58 observed or calculated and disseminated, enabling more objective comparisons among seasons

¹<https://www.sedema.cdmx.gob.mx/>

59 and locations. The UVI observations from Mexico City, considered here, are an important
60 element of this global picture.

61 While the UVI at the surface cannot be translated directly into photolysis frequencies
62 for various photo-labile molecules, the spectral weighting of the UVI (ca. 300-320 nm) is
63 approximately similar to that for the photolysis of ozone to singlet oxygen atoms. Other UV
64 wavelengths are of course also important, e.g. for the photolysis of nitrogen dioxide, and
65 may be affected differently depending on the pollutant. With these considerations and a few
66 other caveats, UVI trends examined here can also be used to infer accompanying trends in
67 photolysis frequencies and influences on photochemical smog formation.

68 Methods

69 Ground-based measurements

70 The Mexico City Metropolitan Area is located at 19.4°N, 99.1°W, 2240 meters above sea
71 level (asl), surrounded by mountain ridges exceeding 5000 m asl, with complex topog-
72 raphy and thermal inversions that inhibit winds and favor intense air pollution.³³⁻³⁵ Air
73 quality monitoring and surface meteorological measurements in the MCMA are conducted
74 continuously by the Automated Atmospheric Monitoring Network (RAMA, by its Spanish
75 acronym) of the Atmospheric Monitoring System (SIMAT, by its Spanish acronym) of the
76 Mexico City government. Since the year 2000, UV radiometers (model 501-A, Solar Light
77 Company Inc., Glenside, PA) detecting wavelengths between 280-400 nm have been mea-
78 suring erythemally-weighted solar radiation. The calibration of the UV sensors has been
79 carried out annually by comparing against a factory-calibrated reference sensor. The out-
80 put voltages from the network's sensors have been compared for at least one week against
81 the UV readings from the reference sensor to derive a calibration factor. New calibration
82 factors typically differ from the old ones by 2% or less. Reference sensors have been also
83 calibrated by the manufacturer and updated periodically (between 3 to 5 years) to reduce

84 systematic errors due to drifts in sensitivity. Long term calibration drift are minimized by
 85 these yearly re-calibrations. Although at the beginning only a few stations were in oper-
 86 ation and have been changing, currently 11 stations are recording erythemal irradiances,
 87 which are then multiplied by 40 (see Eq. 1) to give UV Indices. Table 1 describes the lo-
 88 cation of the stations where the UV Index has been measured. Figure 1 shows how the
 89 radiometers of the SIMAT have been distributed over MCMA, prioritizing sites with higher
 90 population density. Near real-time data for each station are available on the SIMAT official
 91 website <http://www.aire.cdmx.gob.mx/default.php>. Daily maximum values (UVI_{max})
 92 were extracted in each of the stations around solar noon from the time interval from 11:00
 93 h-15:00 h CST (Central Standard Time). This database with 7305 continuous days of mea-
 94 surements during the period 2000-2019 was analyzed.

Table 1: SIMAT stations and AERONET site*, environmental descriptors and geographical positions. Abbreviations names: Chalco (CHA), Cuautitlán (CUT), FES Acatlán (FAC), Hangares (HAN), Laboratorio de Análisis Ambiental (LAA), Merced (MER), Montecillo (MON), Milpa Alta (MPA), Pedregal (PED), San Agustín (SAG), Santa Fe (SFE), Tlalnepantla (TLA) and National Autonomous University of Mexico (UNAM*)

Station	Environment	Lat (°N)	Lon (°W)	El (masl)
CHO	semi-urban	19.27	98.89	2253
CUT	ecological park	19.72	99.20	2263
FAC	urban	19.48	99.24	2299
HAN	urban	19.42	99.08	2235
LAA	urban	19.48	99.15	2255
MER	downtown	19.42	99.12	2245
MON	rural	19.46	98.90	2252
MPA	rural	19.18	98.99	2594
PED	residential	19.33	99.20	2326
SAG	urban	19.53	99.03	2241
SFE	residential	19.36	99.26	2599
TLA	urban	19.53	99.20	2311
UNAM*	University city	19.33	99.18	2294

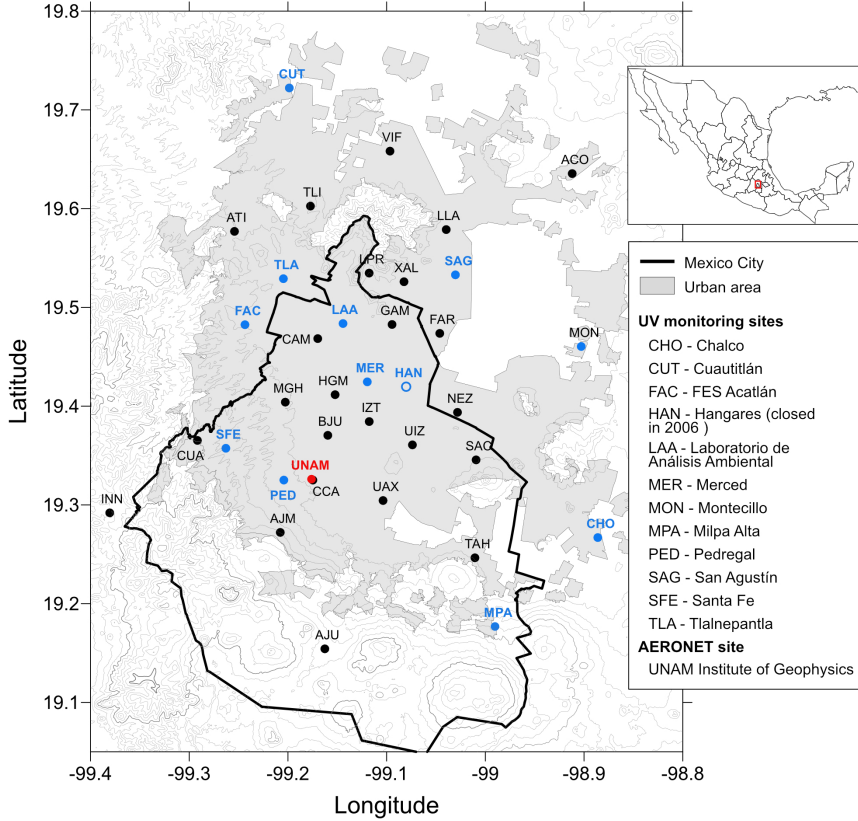


Figure 1: Map with the location of the SIMAT continuous monitoring stations over MCMA. Sites denoted by the blue solid dots correspond to SIMAT stations with UV measurements, while the black dots indicate SIMAT stations without UV measurements, the site indicated by an open blue dot represents a discontinued site, the red dot shows the location of the AERONET site. The location of Mexico City and the acronyms of the UV and AERONET site are shown at the upper and lower frames at the right respectively.

With the aim to explore the relationship between UVI and air pollutants levels, the hourly averages for ozone (O_3), carbon monoxide (CO), nitrogen dioxide (NO_2), sulfur dioxide (SO_2) and particle matter with diameter sizes $\leq 10 \mu m$ (PM_{10}), were downloaded from the SIMAT.³⁶ For purposes of assessing the influence on the UV Index at solar noon, only values obtained between 11h and 15h CST were considered for the trends analysis. Pollutant measurements are conducted by the SIMAT using regulatory-grade commercial instruments. Measurement principles include ultraviolet photometry (model 400E, Teledyne-API) for O_3 , chemiluminescence (model 200E, Teledyne-API) for NO_2 , UV fluorescence (model 100E, Teledyne API) for SO_2 , and infrared absorption (model 300E, Teledyne-API) for CO.

¹⁰⁴ The PM₁₀ continuous mass concentration was measured with Tapered Element Oscillating
¹⁰⁵ Microbalance (TEOM 1400AB or TEOM 1405 DF, Thermo Scientific) monitors. Gaseous
¹⁰⁶ pollutant levels are reported in ppb concentration units for O₃, SO₂ and NO₂, and in ppm
¹⁰⁷ for CO. Particulate matter mass concentration is reported in $\mu\text{g m}^{-3}$ at local conditions for
¹⁰⁸ temperature and pressure.

¹⁰⁹ Aerosol optical depth at 340 nm was obtained from the Institute of Geophysics of the
¹¹⁰ National Autonomous University of Mexico (UNAM). Measurements were conducted with
¹¹¹ a CIMEL sun photometer model CE-318, which is an automatic sun-sky-scanning spectral
¹¹² radiometer of the AErosol RObotic NETwork (AERONET³⁷). The data Product Level 2.0
¹¹³ and 1.5 (only in 2019) were selected, and annual averages AOD₃₄₀ were calculated along
¹¹⁴ the period 2000-2019, except for the year 2011 due to there were no measurements. A
¹¹⁵ previous study of the AOD behavior from 2000 to 2014 demonstrated that data gaps did not
¹¹⁶ significantly change the trends calculated for this.³⁸ Only 8% of the data between the years
¹¹⁷ 2014 and 2019 were missing. The largest data gap occurred in 2018 when the instrument
¹¹⁸ was returned for calibration.

¹¹⁹ Satellite data

¹²⁰ The UV Index data derived from satellite measurements of reflected radiance were used for
¹²¹ comparison with the ground-based measurements. These data were provided by the Ozone
¹²² Monitoring Instrument (OMI) on board of AURA-NASA satellite.³⁹ OMI is operated in co-
¹²³ operation between the Netherlands Agency for Aerospace Programmes (NIVR), the Finnish
¹²⁴ Meteorological Institute (FMI) and NASA. OMI performs observations over a geographical
¹²⁵ dimension of 13×24km² at nadir. For the coordinates (19.33N, 99.18W) and elevation (2268
¹²⁶ masl) of Mexico City, the satellite overpass time is between 19:00h - 21:00h UTC (20:00h
¹²⁷ - 22:00h CET). Measurements of the ozone profile and cloud cover are used via a radiative
¹²⁸ transfer model to estimate the UVI at the ground. The UV Index used for Mexico City
¹²⁹ corresponds to values at local noon time and clear sky from OMUVB Level 2 data product,

130 version 1.3 and collection 3.

131 TUV model

132 Calculations of the UV Index were also made with the Tropospheric Ultraviolet Visible
133 (TUV v5.3) model.⁴⁰ The model atmosphere was represented by 80 vertical layers, each 1
134 km thick, starting at the 2.24 km asl elevation of MCMA, and for which the first three km
135 constitute the atmospheric boundary layer (BL).⁴¹ The ozone profile above the BL is from
136 the US Standard Atmosphere, but rescaled to a value of 259.6 DU. Totals including the BL
137 contributions (of 13.7 DU in the year 2000 and 9.8 DU in 2019, see below) were 273.1 DU
138 in 2000 and 269.2 DU. The climatological O₃ column for this latitude and season is about
139 270 DU (plus or minus ca. 5 DU) so in good agreement with the values used here.

140 Pollutants within the BL (including O₃) are assumed to be well mixed, in agreement with
141 observations from the MILAGRO field campaign that showed the disappearance of vertical
142 gradients in the profiles of gases^{42,43} and aerosols^{44,45} by late morning. The UV-absorbing
143 gases considered here are O₃, NO₂, and SO₂, specified in ppb.

144 BL aerosols are modeled by prescribing the AOD at 340 nm (from AERONET observa-
145 tions), scaled to other wavelengths inversely with wavelength (Angstrom coefficient = 1.0),
146 asymmetry factor of 0.7, and a single scattering albedo of 0.85 at UV wavelengths, following
147 the determinations made in Mexico City by Corr et al.⁴⁶ and Palancar et al.¹².

148 Above the atmospheric boundary layer, the model was taken to be free of aerosols, NO₂,
149 or SO₂. In one sensitivity study, a total AOD of 0.7 was redistributed placing 0.2 in the
150 free troposphere (decreasing vertically with an exponential scale height of 4 km, and 0.5
151 remaining in the BL). The calculated UVI differed by less than 1%. Thus, as long as the
152 total AOD is known, knowledge of the exact vertical aerosol profile is not critical towards
153 ground-level UVI – but would obviously affect the vertical structure of photolysis frequencies.

154 Radiative transfer calculations were carried out with the pseudo-spherical 4-stream op-
155 tion, at 1 nm steps between 280 and 400 nm.

¹⁵⁶ Results and Discussion

¹⁵⁷ Figure 2 shows the diurnal variation of the UVI for several specific cloud-free days, for
¹⁵⁸ different seasons and several locations (CHO, MER, MON, PED, SAG, SFE and TLA).
¹⁵⁹ UV Index from TUV model was used as reference of the behavior under clear sky days.
¹⁶⁰ According to the comparison of measurements minute by minute, the dates with prolonged
¹⁶¹ fluctuations along the day were discarded. However, during the rainy period (from June
¹⁶² to October) at least a brief clouds presence is common, as shown at CHO station around
¹⁶³ noon in 13 June 2017. Peak values range from 8 during autumn/winter to above 12 in
¹⁶⁴ spring/summer, in correspondence to the respective December and June solstices. Although
¹⁶⁵ the stations are all within a 25 km radius, substantial differences among them are notable.
¹⁶⁶ Survey of the locations revealed that shadowing from nearby structures is not an issue. The
¹⁶⁷ good agreement in the morning, followed by more divergence in the afternoon, is consistent
¹⁶⁸ with the development of photo-chemical pollution hotspots during the day. Previous studies
¹⁶⁹ (e.g., Castro et al.⁴⁷ and Palancar et al.¹²) have shown that surface UV radiation in Mexico
¹⁷⁰ City is attenuated significantly by aerosols. The measurements shown in Fig. 2 are consistent
¹⁷¹ with this increasing pollution during the course of the day, with highest aerosol loading (and
¹⁷² highest variability) attained in the afternoon. Further support for the role of pollution in
¹⁷³ suppressing the UVI comes from the observation made at the Santa Fe (SFE) site which in
¹⁷⁴ Fig. 2 are seen to be systematically higher, e.g. by over 10% in autumn afternoons, compared
¹⁷⁵ to the other stations. The SFE station is displaced to the west from the majority of the
¹⁷⁶ other stations, and remains in the outskirts. This site is also approximately 300 m higher
¹⁷⁷ than Mexico City downtown, so that the cleaner atmosphere results from both vertical and
¹⁷⁸ horizontal variations in pollution levels.⁴⁸ It is indeed expected to have higher values of the
¹⁷⁹ UVI, in agreement with the observations.

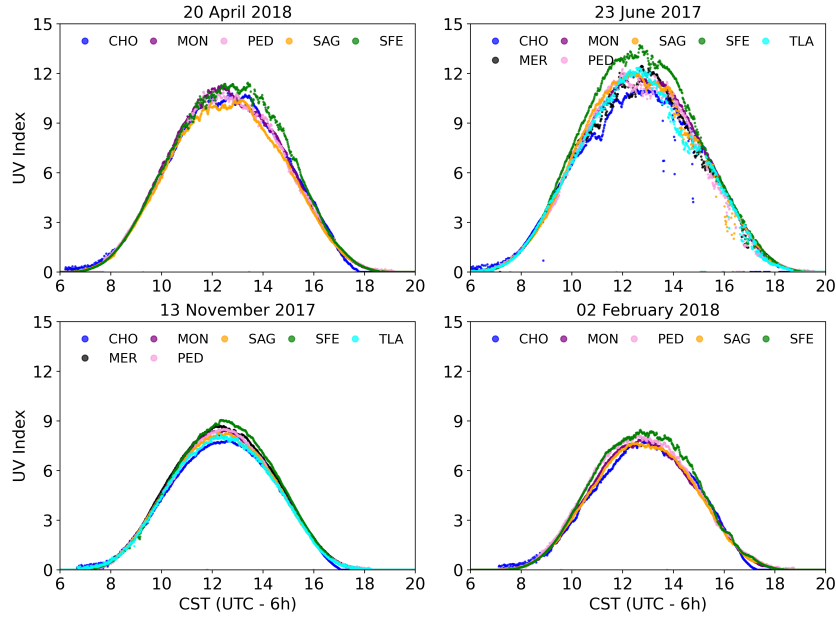


Figure 2: UV Index measured over MCMA by SIMAT stations each minute along the day under practically cloudless conditions for representative days of the year.

180 The daily maximum UV Index of each station is denoted by UVI_{max} , all of them were

181 counted in the period 2000-2019. As shown in Figure 3, these values ranged from 1 to

182 16, with a majority (61%) of the days experienced UVI_{max} values between 6 and 10, and

183 remarkably few, less than 1%, in the higher 13-16 range. The lowest values are likely due to

184 winter days with heavy cloud cover and low sun angles, and UV attenuation by pollutants

185 could also be amplified under such conditions, due to longer photon path lengths at low sun

186 and within clouds. The extreme sparsity of high UVI values remains surprising, and may be

187 an indication of the rarity of extremely unpolluted days within the city.

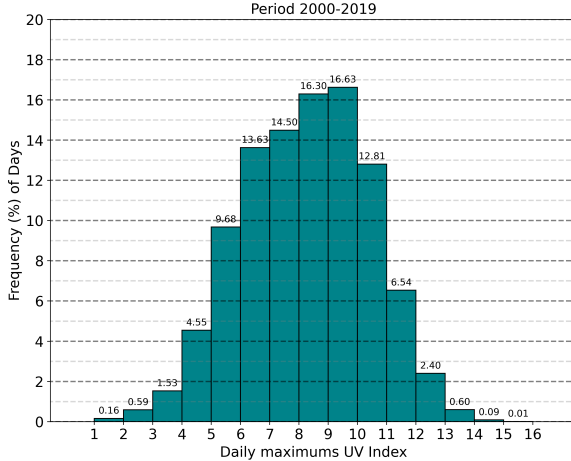


Figure 3: Frequency distribution of daily maximum UV Index values in Mexico City during 2000 -2019.

188 Similar patterns are found when considering the monthly average of the UVI_{max} values
 189 as shown in Figure 4. The long-term averages present a seasonal variation (as in Fig. 2)
 190 that follows approximately the cosine of the noontime solar zenith angle. Notably, values
 191 rarely if ever exceed 12 (as in Fig. 3). The lowest average UVI (near 7) take place in winter
 192 while from March to August the values seem to be flattened in the range 10-11. The rather
 193 low monthly UV Index values, mainly could be a consequence of the presence of clouds in
 194 the rainy season. However, urban aerosol pollution sources, biomass burning for agriculture
 195 and wood cooking also contribute to poor air quality between March-May⁴⁹. Using the
 196 maximum UVI_{max} from all of stations every day (one daily point), the monthly averages
 197 (\overline{UVI}_m) were calculated along the period 2000-2019 (except for June 2003 due to there were
 198 no measurements). Long term trends in \overline{UVI}_m are shown in Figure 5. A clear upward trend
 199 is seen, with a slope for the linear fit of 0.9%/year or +1.5 UVI units over the two decades.

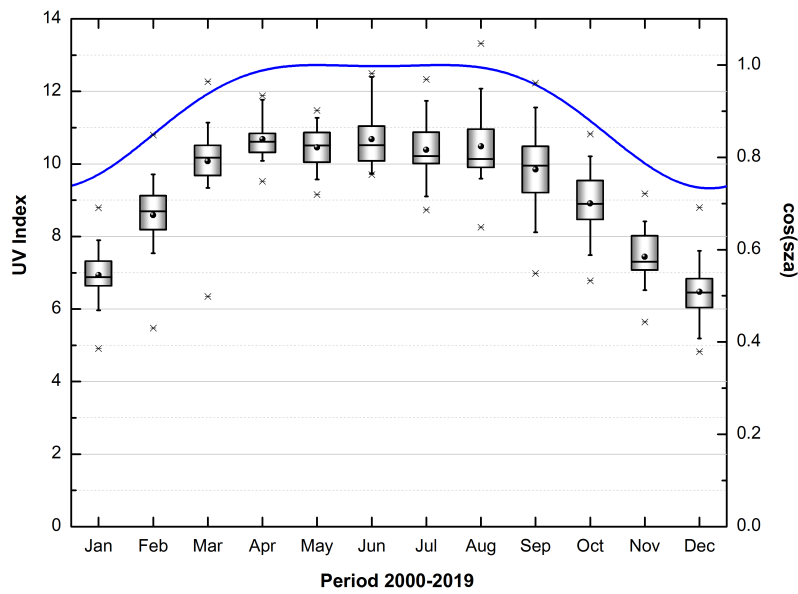


Figure 4: Boxplot of the monthly averages of the maximum UV Index values (black dot) in MCMA for the period 2000-2019: median (central bold line), standard deviation (box edges), 25th and 75th percentiles (the whiskers), the minimum and maximum values (plus sign) and the cosine of the solar zenith angle at solar noon (blue curve).

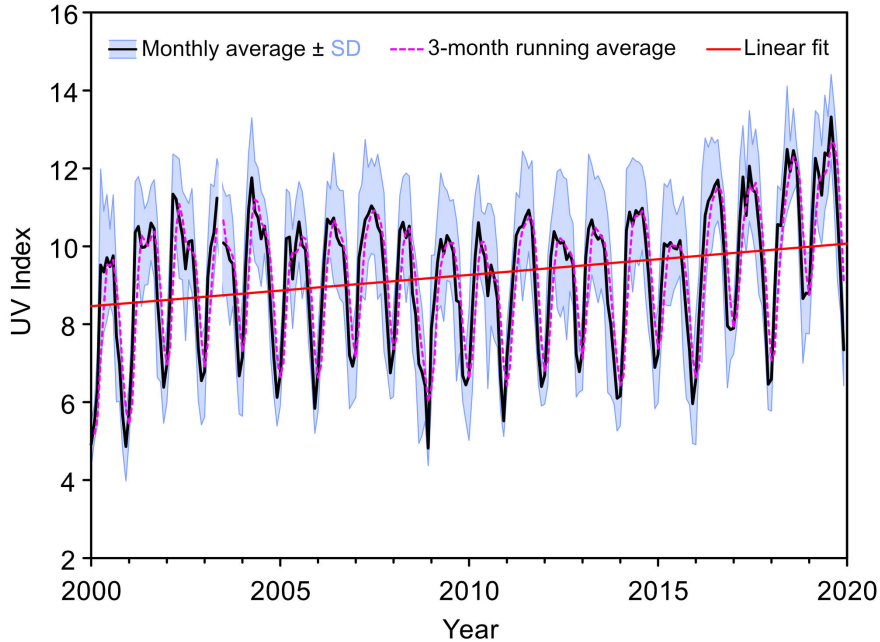


Figure 5: Moving average function (light gray curve) quarterly applied to monthly average UV Index, standard deviation of all data within a given month (black dots and dash line) and linear fit (red line).

200 The UV Index computed from satellite-based observations over the period 2005-2019 is

201 mapped in Figure 6. The satellite-derived UVIs vary from 8 in winter to 16 in summer, both

202 values being substantially higher than the ground-based observations (ca. 7 for winter and

203 11 for summer, see Fig. 4). We hypothesize that this large difference between satellite-based

204 estimation and ground-based observation of the UV index is due to the intense air pollution

205 of Mexico City. A rather similar behavior was detected in Santiago city, Chile.⁵⁰

206 Close inspection of Figure 6 shows that the maximum values are reached in June and

207 July of each year. While the early OMI estimates of the UVI did not account for the

208 boundary layer aerosol absorption, the current version (1.3) includes the postcorrection by

209 Arola et al.⁵¹ for absorbing aerosols based on global monthly aerosol climatology.

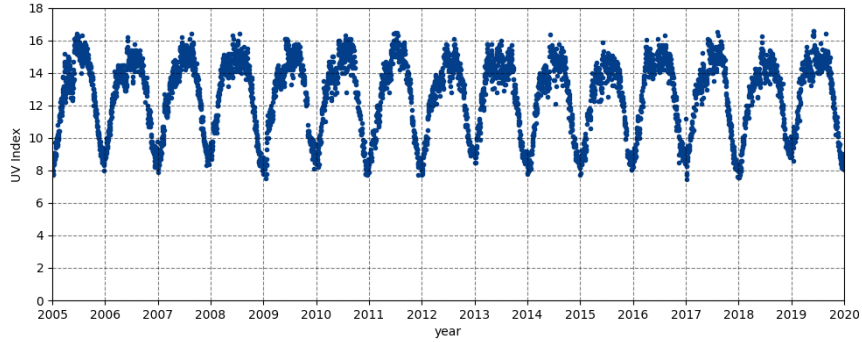


Figure 6: UV Index at solar noon for clear sky recorded by OMI-Aura/NIVR-FMI-NASA, from 2005 to 2019.

²¹⁰ Effect of pollutants on UV radiation

²¹¹ Trends and averages in aerosol optical depth AOD_{340} and criteria pollutants PM_{10} , CO,
²¹² NO_2 , O_3 and SO_2 observed at the SIMAT stations over 2000-2019, are shown in Figure 7
²¹³ and summarized in Table 2 together with the UVI_{max} . Similar trends in pollutants have
²¹⁴ been noted before^{48,52,53} and reflect the long-term success of emission reduction policies and
²¹⁵ programs.

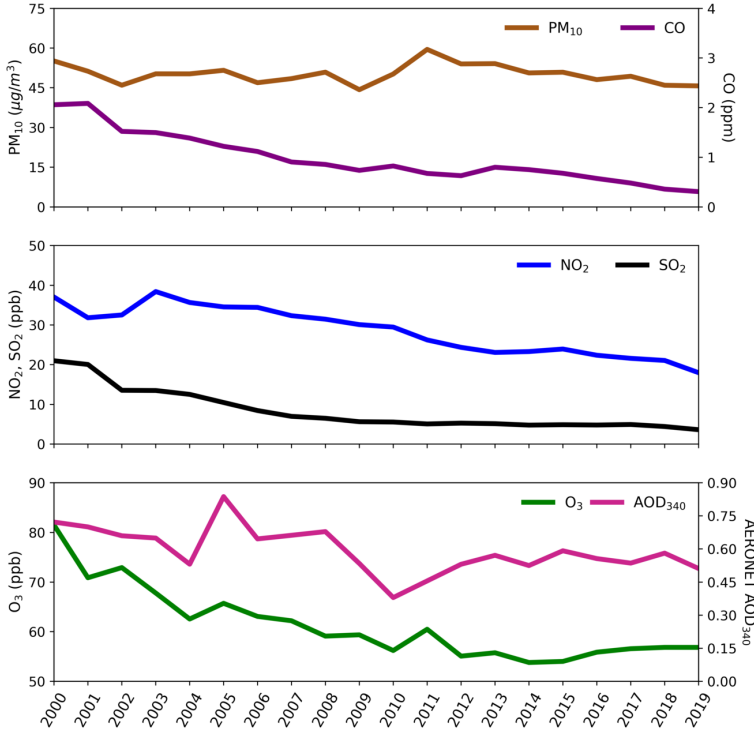


Figure 7: Air quality trends in MCMA for the period 2000-2019 from annual averages obtained between 11h to 15h CST every day: PM₁₀ (brown curve), CO (purple curve), NO₂ (blue curve), SO₂(black curve), O₃ (green curve) and AOD₃₄₀ (pink curve).

Table 2: UV Index and criteria pollutants: the absolute change per year for the period 2000-2019, averages in units of $\mu\text{g}/\text{m}^3$ (PM₁₀), ppm (CO), ppb (SO₂, NO₂ and O₃), dimensionless (UV Index and AOD₃₄₀) and annual percentage change (%/year).

Variable	$\frac{\text{absolutechange}}{\text{year}}$	Avg _{2000–2019}	$\Delta(\%/\text{year})$
UVI	0.08	9.2	0.9
PM ₁₀	-0.10	50.2	-0.2
CO	-0.08	1.0	-8.2
NO ₂	-0.96	28.6	-3.4
O ₃	-1.05	61.3	-1.7
AOD ₃₄₀	-0.01	0.6	-1.6
SO ₂	-0.76	8.4	-9.1

The observed changes in the concentrations of these air pollutants have significant implications for surface UV radiation, as can be demonstrated with the TUV radiative transfer model. Table 3 summarizes UVI values for the June-July time period, estimated by the

219 three methods: OMI satellite-derived UVI, RAMA ground-based observations, and TUV
 220 modeling using air pollution estimates. Two groups of values can be readily identified: (1)
 221 RAMA daily record values, OMI with or without BL aerosols, and TUV for very clean con-
 222 ditions, all with UVI values around 15-16; and (2) RAMA average daily maxima and TUV
 223 UVI using MCMA pollutants as input, which are in good agreement for both 2018/19 and
 224 2000/01 but much lower than the first group. Compared to the OMI estimate that included
 225 the climatological aerosol correction (15.3), observed RAMA values were lower by 35% in
 226 2000 and by 20% in 2019. Similarly, TUV values were 35% lower in 2000 and 22% lower in
 227 2019 relative to the TUV values of 15.6 for a pristine atmosphere.

Table 3: UV Index monthly maximum estimates for June-July.

Conditions for estimation in June-July	UV Index
RAMA maximum reached in period 2000-2019	15.0
RAMA average maxima 2018, 2019	12.3
RAMA average maxima 2000, 2001	9.9
OMI clear, local noon, no corrected for BL aerosols	16.6
TUV "zero" pollution	16.1
AOD 0, O ₃ 0 ppb, NO ₂ 0 ppb, SO ₂ 0 ppb	
TUV pristine pollution	15.6
AOD 0.05, O ₃ 10 ppb, NO ₂ 0 ppb, SO ₂ 0 ppb	
TUV 2019:	12.1
AOD 0.5, O ₃ 50 ppb, NO ₂ 20 ppb, SO ₂ 1 ppb	
TUV 2000:	10.2
AOD 0.7, O ₃ 70 ppb, NO ₂ 40 ppb, SO ₂ 20 ppb	

228 The agreement between RAMA observations and TUV model estimates is excellent but
 229 also probably a bit fortuitous. Clouds on average reduce the irradiance impinging on the
 230 surface, but scattering from them can also cause transient enhancements (especially if the
 231 direct sunbeam is not blocked) that could be recorded as daily maxima – with cancellation
 232 between these cloud effects resulting in improved agreement with the cloud-free model. We
 233 cannot exclude that some of the observed trend in UVI is due to changes in cloud cover.
 234 However, the modeled fractional UVI reductions due to pollutants, shown in Table 3, are in
 235 such good agreement with the observed UVI reductions, that a compelling case can be made

236 for a dominant role of air pollutants in the long-term UVI trends.

237 Table 4 shows the contributions to UVI reductions from individual pollutants. Aerosols
238 are seen to be the major factor in both time periods, followed by O₃, NO₂, and SO₂. The
239 2000-2019 UVI increase is seen to result in comparable proportions from fewer aerosols, less
240 SO₂, and the combined reductions in O₃ and NO₂.

241 Comparable UV reductions, of 30-40% due to aerosols, were reported by Panicker et al.¹¹
242 over Pune, India from April 2004 to March 2005, with sensitivity coefficients (i.e. change in
243 UVI per unit change in AOD) similar to those found here in Table 3.

244 Comparisons of OMI with ground-based UV measurements have been reviewed recently
245 by Zhang et al.⁵⁴ and Vitt et al.⁵⁵. OMI-derived UV generally overestimates ground-level
246 measurements by 1-10% in relatively clean conditions (e.g. rural U.S), by 10-30% in Southern
247 Europe and by 40% or more in Santiago, Chile⁵⁰ and Thailand⁵⁶. The overestimations appear
248 related in large part to incomplete accounting of UV absorption by BL aerosol, although
249 other factors such as the correction to solar noon may also introduce some bias.⁵⁴ Over
250 Europe, ground-based UVI observations for several decades are systematically lower than
251 those estimated from satellites even after consideration of climatological aerosol distributions,
252 showing the importance of local pollution not resolved from space.⁵⁵ However, difference
253 between satellite-derived and ground-based UVI was less than 1.0 UVI units in over 90% of
254 the cases, in contrast to the difference of 3-5 units found for Mexico City (Table 3).

255 UV reductions by air pollutants are expected to be most severe near the surface, while
256 chemical reactions leading to photochemical smog occur through the vertical extent of the
257 BL. Figure 8 shows the vertical profiles of photolysis coefficients (the reciprocals of photolytic
258 lifetimes) for two key reactions, the photolysis of O₃ to yield excited oxygen atoms O(1D),
259 and the photolysis of NO₂. In the absence of optically active pollutants, these coefficients
260 would be nearly independent of altitude in the BL. However, the presence of pollutants
261 leads to a strong decrease toward the surface, with notably more severe reductions in 2000
262 compared to 2019. While the specific values shown in the figure are only illustrative for

263 typical conditions, routine daily air quality modeling should carefully account for the long
 264 term variations in these photolysis coefficients.

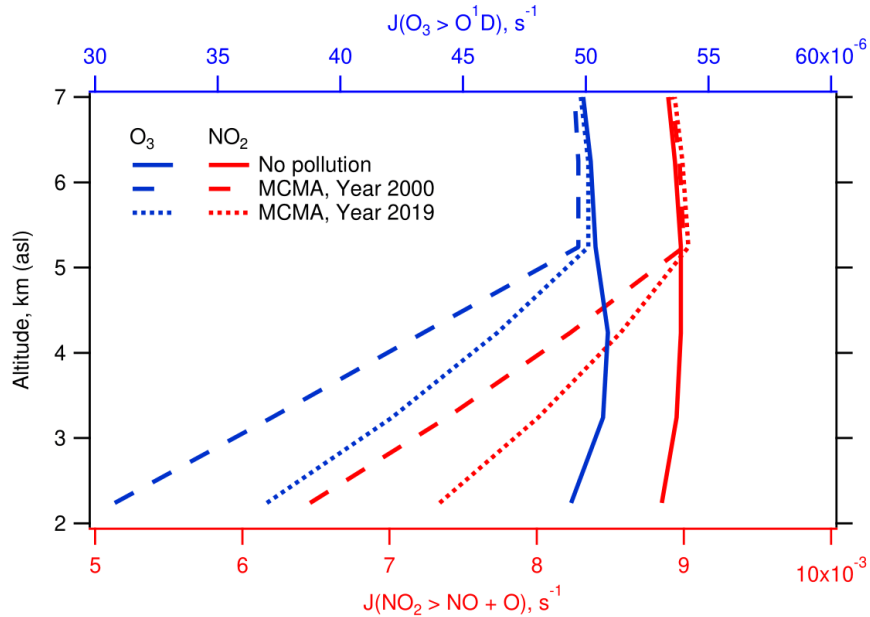


Figure 8: Vertical profiles of the photolysis coefficients for the reaction $O_3+h\nu \rightarrow O(1D)+O_2$ (top axis, blue) $NO_2+h\nu \rightarrow O+NO$ (bottom axis, red) for zero pollution (solid) and Mexico City in the years 2000 (dashed) and 2019 (dotted)

265 An issue that is beginning to gain relevance in radiative balance models is the influence
 266 of a group of organic compounds capable of strongly absorbing in the UV region (brown
 267 carbon).⁵⁷ Some of these compounds are related with emissions from local and regional
 268 wildfires.⁵⁸ Mexico City is frequently exposed to regional fire smoke transport during the
 269 dry part of the year (November to May)⁵⁹, that sporadically modify the optical properties of
 270 the aerosols.⁶⁰ This could partly explain the relatively minor reductions in PM_{10} (see Fig. 7),
 271 compared to the larger reductions of CO , NO_2 , and O_3 that are more directly related to urban
 272 activities, as well as some of the seasonal asymmetry seen in Fig. 3.

273 The UVI is specific to wavelengths mainly in the 300-320 nm range, and so the question
 274 remains whether these results can be applied at longer UV wavelengths, e.g. those important
 275 for NO_2 photolysis (<420 nm). Absorption by SO_2 and O_3 vanishes, while absorption by NO_2
 276 increases and typical aerosols optical depth decrease. These changes can easily be modeled,

²⁷⁷ but unfortunately far fewer measurements of these longer wavelengths are available in Mexico
²⁷⁸ City or elsewhere.

²⁷⁹ Two decades of observations in Mexico City demonstrate unequivocally that air pollution
²⁸⁰ reduces UV radiation at the ground. The ground-based observations are well below data
²⁸¹ derived from satellite-based observations. Although ideally both data sets should match,
²⁸² the satellite has a limitation to seeing boundary layer absorbers. When typical values of the
²⁸³ pollutants (aerosols, tropospheric ozone, and to a lesser extent NO₂ and SO₂), are included
²⁸⁴ in a model (e.g. TUV), the differences between satellite-derived and ground-based measured
²⁸⁵ values are explained and can be attributed quantitatively to individual observed pollutants.
²⁸⁶ Long term improvements in air quality, over two decades, are accompanied by statistically
²⁸⁷ significant increases in the observed UVI, again in good agreement with the model-predicted
²⁸⁸ changes.

Table 4: Contributions of individual pollutants to UV Index changes. (a) Values used one at the time, with the others held at zero. (b) UVI deviation from the zero-pollution value of 16.1 (from Table 3). (c) 2019-2000 UVI change due to changes in each pollutant.

Pollutant	Year 2000		Year 2019		2019-2000
	poll. level (a)	UVI (b)	poll. level	UVI	(c)
AOD	0.7	-3.7	0.5	-2.7	1.0
O ₃ ppb (DU)	70 (14)	-1.4	50 (10)	-1.0	0.4
NO ₂ ppb	40	-0.9	20	-0.5	0.4
SO ₂ ppb	30	-0.8	1	-0.04	0.8

²⁸⁹ The reductions in surface UV radiation with respect to an ideally clear atmosphere –
²⁹⁰ by nearly 40% in 2000 and still 20% in 2020 – are large, both within the context of hu-
²⁹¹ man UV exposure and air quality mitigation. In urban areas where ozone production scales
²⁹² proportionally with UV levels and with volatile organic compound (VOC) emissions (the
²⁹³ VOC-limited regime), a 10% increase in BL average photolysis rates means that VOC emis-
²⁹⁴ sions will need to be reduced by 10% to meet the same goals, or else successful reductions in
²⁹⁵ aerosols would lead to unwanted UV-driven increases in O₃. Such UV changes must be con-
²⁹⁶ sidered carefully in air quality mitigation strategies. For human exposure, a 20% increase in

297 UV irradiances over two decades should be seen as a non-negligible public health issue requir-
298 ing some reassessment of preventive behaviors to minimize the risk of skin cancer, cataract,
299 and other UV-related health effects. The efforts that Mexico City has made to improve air
300 quality have achieved positive results in the levels of most air pollutants. Nevertheless, they
301 caused an increase in UV radiation that reaches the surface.

302 A limitation of the present work is our focus on daily maximum values, which largely
303 exclude cloud cover. Absorption within clouds can be enhanced by the long path lengths of
304 multiply scattered photons, so that accurate quantification of UV effects of clouds in polluted
305 environments remains a significant challenge and interesting opportunity for future work.

306 Finally, based on our results, the solar radiation monitoring network could be improved
307 by adding observation sites within or close to the basin, with minor influences of the urban
308 plume (e. g., Amecameca; latitude: 19.13°N, longitude: 99.76°W, elevation: 2420 m asl),
309 and the complementing of sensors in existing monitoring sites that are at elevations above the
310 urban boundary layer like Ajusco (AJU, elevation: 2953 m asl) or Instituto de Investigaciones
311 Nucleares (INN, elevation: 3082 m asl). These sites would provide valuable observations to
312 assess quantitatively the effects of urban pollution on solar radiation levels.

313 Acknowledgement

314 We wish to acknowledge the staff of SIMAT, from the Secretariat of Environment, for the
315 data and the continuous assistance during the realization of this project. Adriana Ipiña would
316 like to extend her thanks to Dirección General de Personal Académico, Universidad Nacional
317 Autónoma de México (DGAPA-UNAM) for the postdoctoral fellowship at Centro de Ciencias
318 de la Atmósfera of the UNAM. Rubén D Piacentini wishes to thank CONICET and National
319 University of Rosario, Argentina, for their partial support to the present work. The National
320 Center for Atmospheric Research is sponsored by the National Science Foundation.

321 **References**

- 322 (1) Taylor, H. R.; West, S. K.; Rosenthal, F. S.; Muñoz, B.; Newland, H. S.; Abbey, H.;
323 Emmett, E. A. Effect of Ultraviolet Radiation on Cataract Formation. *New England
324 Journal of Medicine* **1988**, *319*, 1429–1433.
- 325 (2) Varotsos, C.; Feretis, E. Health effects on human eye resulting from the increased
326 ambient solar ultraviolet radiation. *Toxicological & Environmental Chemistry* **1997**,
327 *61*, 43–68.
- 328 (3) Lucas, R. M.; Yazar, S.; Young, A. R.; Norval, M.; de Gruijl, F. R.; Takizawa, Y.;
329 Rhodes, L. E.; Sinclair, C. A.; Neale, R. E. Human health in relation to exposure to solar
330 ultraviolet radiation under changing stratospheric ozone and climate. *Photochemical &
331 Photobiological Sciences* **2019**, *18*, 641–680.
- 332 (4) Leighton, P. A. *Photochemistry of Air Pollution*; Elsevier, 1961; pp v–vi.
- 333 (5) Seinfeld, J. H.; Pandis, S. N.; Noone, K. Atmospheric Chemistry and Physics: From
334 Air Pollution to Climate Change. *Physics Today* **1998**, *51*, 88–90.
- 335 (6) Finlayson-Pitts, B. J.; Pitts, J. N. *Chemistry of the Upper and Lower Atmosphere*;
336 Academic Press, 2000; pp xvii–xviii.
- 337 (7) Liu, S. C.; McKeen, S. A.; Madronich, S. Effect of anthropogenic aerosols on biologically
338 active ultraviolet radiation. *Geophysical Research Letters* **1991**, *18*, 2265–2268.
- 339 (8) Sabziparvar, A. A.; Forster, P. M. F.; Shine, K. P. Changes in ultraviolet radiation due
340 to stratospheric and tropospheric ozone changes since preindustrial times. *Journal of
341 Geophysical Research: Atmospheres* **1998**, *103*, 26107–26113.
- 342 (9) Madronich, S.; Wagner, M.; Groth, P. Influence of Tropospheric Ozone Control on
343 Exposure to Ultraviolet Radiation at the Surface. *Environmental Science & Technology*
344 **2011**, *45*, 6919–6923.

- 345 (10) McKenzie, R. L.; Weinreis, C.; Johnston, P. V.; Liley, B.; Shiona, H.; Kotkamp, M.;
346 Smale, D.; Takegawa, N.; Kondo, Y. Effects of urban pollution on UV spectral irradi-
347 ances. *Atmospheric Chemistry and Physics* **2008**, *8*, 5683–5697.
- 348 (11) Panicker, A. S.; Pandithurai, G.; Takamura, T.; Pinker, R. T. Aerosol effects in the
349 UV-B spectral region over Pune an urban site in India. *Geophysical Research Letters*
350 **2009**, *36*, L10802 1–5.
- 351 (12) Palancar, G. G.; Lefer, B. L.; Hall, S. R.; Shaw, W. J.; Corr, C. A.; Herndon, S. C.;
352 Slusser, J. R.; Madronich, S. Effect of aerosols and NO₂ concentration on ultraviolet
353 actinic flux near Mexico City during MILAGRO: measurements and model calculations.
354 *Atmospheric Chemistry and Physics* **2013**, *13*, 1011–1022.
- 355 (13) Bais, A. F.; McKenzie, R. L.; Bernhard, G.; Aucamp, P. J.; Ilyas, M.; Madronich, S.;
356 Tourpali, K. Ozone depletion and climate change: impacts on UV radiation. *Photo-
357 chemical & Photobiological Sciences* **2015**, *14*, 19–52.
- 358 (14) Hollaway, M.; Wild, O.; Yang, T.; Sun, Y.; Xu, W.; Xie, C.; Whalley, L.; Slater, E.;
359 Heard, D.; Liu, D. Photochemical impacts of haze pollution in an urban environment.
360 *Atmospheric Chemistry and Physics* **2019**, *19*, 9699–9714.
- 361 (15) Li, K.; Jacob, D. J.; Liao, H.; Shen, L.; Zhang, Q.; Bates, K. H. Anthropogenic drivers
362 of 2013–2017 trends in summer surface ozone in China. *Proceedings of the National
363 Academy of Sciences* **2018**, *116*, 422–427.
- 364 (16) Wang, Y. et al. *Contrasting trends of PM2.5 and surface-ozone concentrations in China
365 from 2013 to 2017*; Oxford University Press (OUP), 2020; Vol. 7; pp 1331–1339.
- 366 (17) Wang, W.; Li, X.; Shao, M.; Hu, M.; Zeng, L.; Wu, Y.; Tan, T. The impact of aerosols
367 on photolysis frequencies and ozone production in Beijing during the 4-year period
368 2012–2015. *Atmospheric Chemistry and Physics* **2019**, *19*, 9413–9429.

- 369 (18) Gao, J.; Li, Y.; Zhu, B.; Hu, B.; Wang, L.; Bao, F. What have we missed when studying
370 the impact of aerosols on surface ozone via changing photolysis rates? *Atmospheric*
371 *Chemistry and Physics* **2020**, *20*, 10831–10844.
- 372 (19) Bauwens, M.; Compernolle, S.; Stavrakou, T.; Müller, J.-F.; Gent, J.; Eskes, H.; Lev-
373 elt, P. F.; A, R.; Veefkind, J. P.; Vlietinck, J.; Yu, H.; Zehner, C. Impact of coronavirus
374 outbreak on NO₂ pollution assessed using TROPOMI and OMI observations. **2020**,
375 *47*, e2020GL087978.
- 376 (20) Venter, Z. S.; Aunan, K.; Chowdhury, S.; Lelieveld, J. COVID-19 lockdowns cause
377 global air pollution declines. *Proceedings of the National Academy of Sciences* **2020**,
378 *117*, 18984–18990.
- 379 (21) Shi, X.; Brasseur, G. P. The Response in Air Quality to the Reduction of Chinese
380 Economic Activities During the COVID-19 Outbreak. *Geophysical Research Letters*
381 **2020**, *47*, e2020GL088070.
- 382 (22) Le, T.; Wang, Y.; Liu, L.; Yang, J.; Yung, Y. L.; Li, G.; Seinfeld, J. H. Unexpected air
383 pollution with marked emission reductions during the COVID-19 outbreak in China.
384 *Science* **2020**, *369*, 702–706.
- 385 (23) Red Automática de Monitoreo Atmosférico (RAMA). <http://www.aire.cdmx.gob.mx/descargas/datos/excel/RAMA.xls.pdf>.
- 386 (24) Doran, J. C. et al. The IMADA-AVER Boundary Layer Experiment in the Mexico City
387 Area. *Bulletin of the American Meteorological Society* **1998**, *79*, 2497–2508.
- 388 (25) Molina, L. T.; Kolb, C. E.; de Foy, B.; Lamb, B. K.; Brune, W. H.; Jimenez, J. L.;
389 Ramos-Villegas, R.; Sarmiento, J.; Paramo-Figueroa, V. H.; Cardenas, B.; Gutierrez-
390 Avedoy, V.; Molina, M. J. Air quality in North America's most populous city – overview
391 of the MCMA-2003 campaign. *Atmospheric Chemistry and Physics* **2007**, *7*, 2447–2473.

- 393 (26) Molina, L. T. et al. An overview of the MILAGRO 2006 Campaign: Mexico City
394 emissions and their transport and transformation. *Atmospheric Chemistry and Physics*
395 **2010**, *10*, 8697–8760.
- 396 (27) Jazcilevich, A. D.; García, A. R.; Caetano, E. Locally induced surface air confluence
397 by complex terrain and its effects on air pollution in the valley of Mexico. *Atmospheric*
398 *Environment* **2005**, *39*, 5481–5489.
- 399 (28) Tie, X.; Madronich, S.; Li, G.; Ying, Z.; Zhang, R.; Garcia, A. R.; Lee-Taylor, J.; Liu, Y.
400 Characterizations of chemical oxidants in Mexico City: A regional chemical dynamical
401 model (WRF-Chem) study. *Atmospheric Environment* **2007**, *41*, 1989–2008.
- 402 (29) Zhang, Y.; Dubey, M. K.; Olsen, S. C.; Zheng, J.; Zhang, R. Comparisons of
403 WRF/Chem simulations in Mexico City with ground-based RAMA measurements dur-
404 ing the 2006-MILAGRO. *Atmospheric Chemistry and Physics* **2009**, *9*, 3777–3798.
- 405 (30) Zavala, M.; Brune, W. H.; Velasco, E.; Retama, A.; Cruz-Alavez, L. A.; Molina, L. T.
406 Changes in ozone production and VOC reactivity in the atmosphere of the Mexico City
407 Metropolitan Area. *Atmospheric Environment* **2020**, *238*, 117747.
- 408 (31) WHO,; WMO,; UNEP,; ICNIRP, *Global solar UV index : a practical guide*; 2002; pp A
409 joint recommendation of the World Health Organization, World Meteorological Orga-
410 nization, United Nations Environment Programme, and the International Commission
411 on Non-Ionizing Radiation Protection.
- 412 (32) Webb, A. R.; Slaper, H.; Koepke, P.; Schmalwieser, A. W. Know Your Standard: Clari-
413 fying the CIE Erythema Action Spectrum. *Photochemistry and Photobiology* **2011**, *87*,
414 483–486.
- 415 (33) Whiteman, C. D.; Zhong, S.; Bian, X.; Fast, J. D.; Doran, J. C. Boundary layer evo-
416 lution and regional-scale diurnal circulations over the Mexican plateau. *Journal of*
417 *Geophysical Research: Atmospheres* **2000**, *105*, 10081–10102.

- 418 (34) Fast, J. D.; de Foy, B.; Rosas, F. A.; Caetano, E.; Carmichael, G.; Emmons, L.;
419 McKenna, D.; Mena, M.; Skamarock, W.; Tie, X.; Coulter, R. L.; Barnard, J. C.;
420 Wiedinmyer, C.; Madronich, S. A meteorological overview of the MILAGRO field cam-
421 paigns. *Atmospheric Chemistry and Physics* **2007**, *7*, 2233–2257.
- 422 (35) Carreón-Sierra, S.; Salcido, A.; Castro, T.; Celada-Murillo, A.-T. Cluster Analysis of
423 the Wind Events and Seasonal Wind Circulation Patterns in the Mexico City Region.
424 *Atmosphere* **2015**, *6*, 1006–1031.
- 425 (36) Sistema de Monitoreo Atmosférico,Ciudad de México. <http://www.aire.cdmx.gob.mx/default.php?opc=%27aKBhnml=%27&opcion=Zg>, Accessed on Wed, December 02,
426 2020.
- 427 (37) Holben, B.; Eck, T.; Slutsker, I.; Tanré, D.; Buis, J.; Setzer, A.; Vermote, E.; Reagan, J.;
428 Kaufman, Y.; Nakajima, T.; Lavenu, F.; Jankowiak, I.; Smirnov, A. AERONET—A
429 Federated Instrument Network and Data Archive for Aerosol Characterization. *Remote
430 Sensing of Environment* **1998**, *66*, 1–16.
- 431 (38) Carabali, G.; Estévez, H. R.; Valdés-Barrón, M.; Bonifaz-Alfonzo, R.; Riveros-
432 Rosas, D.; Velasco-Herrera, V. M.; Vázquez-Gálvez, F. A. Aerosol climatology over
433 the Mexico City basin: Characterization of optical properties. *Atmospheric Research*
434 **2017**, *194*, 190–201.
- 435 (39) NASA EOS/Aura Validation Data Center (AVDC) - Correlative data, Field of
436 View Predictions, Data Subsets, GEOMS, DCIO. https://avdc.gsfc.nasa.gov/pub/most_popular/overpass/OMI/.
- 437 (40) Madronich, S. Intercomparison of NO₂ photodissociation and U.V. Radiometer Mea-
438 surements. *Atmospheric Environment* **1987**, *21*, 569–578.
- 439 (41) Shaw, W. J.; Pekour, M. S.; Coulter, R. L.; Martin, T. J.; Walters, J. T. The daytime

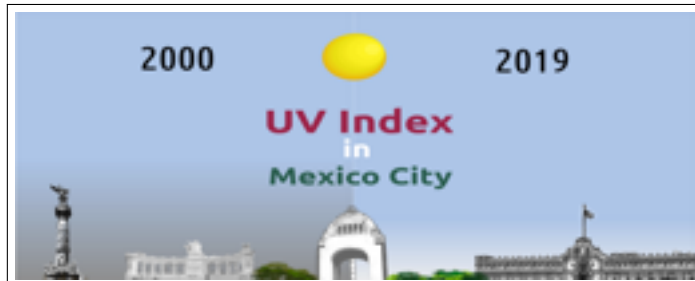
- 442 mixing layer observed by radiosonde profiler, and lidar during MILAGRO. *Atmospheric*
443 *Chemistry and Physics Discussions* **2007**, *7*, 15025–15065.
- 444 (42) Velasco, E.; Márquez, C.; Bueno, E.; Bernabé, R. M.; Sánchez, A.; Fentanes, O.; Wöhrn-
445 schimmel, H.; Cárdenas, B.; Kamilla, A.; Wakamatsu, S.; Molina, L. T. Vertical dis-
446 tribution of ozone and VOCs in the low boundary layer of Mexico City. *Atmospheric*
447 *Chemistry and Physics* **2008**, *8*, 3061–3079.
- 448 (43) Greenberg, J.; Guenther, A.; Turnipseed, A. Tethered balloon-based soundings of ozone
449 aerosols, and solar radiation near Mexico City during MIRAGE-MEX. *Atmospheric*
450 *Environment* **2009**, *43*, 2672–2677.
- 451 (44) Rogers, R. R.; Hair, J. W.; Hostetler, C. A.; Ferrare, R. A.; Obland, M. D.; Cook, A. L.;
452 Harper, D. B.; Burton, S. P.; Shinozuka, Y.; McNaughton, C. S.; Clarke, A. D.; Re-
453 demann, J.; Russell, P. B.; Livingston, J. M.; Kleinman, L. I. NASA LaRC airborne
454 high spectral resolution lidar aerosol measurements during MILAGRO: observations
455 and validation. *Atmospheric Chemistry and Physics* **2009**, *9*, 4811–4826.
- 456 (45) Lewandowski, P. A.; Eichinger, W. E.; Holder, H.; Prueger, J.; Wang, J.; Kleinman, L. I.
457 Vertical distribution of aerosols in the vicinity of Mexico City during MILAGRO-2006
458 Campaign. *Atmospheric Chemistry and Physics* **2010**, *10*, 1017–1030.
- 459 (46) Corr, C. A.; Krotkov, N.; Madronich, S.; Slusser, J. R.; Holben, B.; Gao, W.; Flynn, J.;
460 Lefer, B.; Kreidenweis, S. M. Retrieval of aerosol single scattering albedo at ultraviolet
461 wavelengths at the T1 site during MILAGRO. *Atmospheric Chemistry and Physics*
462 **2009**, *9*, 5813–5827.
- 463 (47) Castro, T.; Madronich, S.; Rivale, S.; Muhlia, A.; Mar, B. The influence of aerosols on
464 photochemical smog in Mexico City. *Atmospheric Environment* **2001**, *35*, 1765–1772.
- 465 (48) Secretaría del Medio Ambiente de la Ciudad de México, *Calidad del aire en la Ciudad*
466 *de México, informe 2017*; 2018; pp 1–160.

- 467 (49) Retama, A.; Baumgardner, D.; Raga, G. B.; McMeeking, G. R.; Walker, J. W. Sea-
468 sonal and diurnal trends in black carbon properties and co-pollutants in Mexico City.
469 *Atmospheric Chemistry and Physics* **2015**, *15*, 9693–9709.
- 470 (50) Cabrera, S.; Ipiña, A.; Damiani, A.; Cordero, R. R.; Piacentini, R. D. UV index values
471 and trends in Santiago Chile (33.5°S) based on ground and satellite data. *Journal of*
472 *Photochemistry and Photobiology B: Biology* **2012**, *115*, 73–84.
- 473 (51) Arola, A. et al. A new approach to correct for absorbing aerosols in OMI UV. *Geophys-
474 ical Research Letters* **2009**, *36*, L22805 1–5.
- 475 (52) Parrish, D. D.; Singh, H. B.; Molina, L.; Madronich, S. Air quality progress in North
476 American megacities: A review. *Atmospheric Environment* **2011**, *45*, 7015–7025.
- 477 (53) Molina,; Velasco,; Retama,; Zavala, Experience from Integrated Air Quality Manage-
478 ment in the Mexico City Metropolitan Area and Singapore. *Atmosphere* **2019**, *10*,
479 512.
- 480 (54) Zhang, H.; Wang, J.; García, L. C.; Zeng, J.; Dennhardt, C.; Liu, Y.; Krotkov, N. A.
481 Surface erythemal UV irradiance in the continental United States derived from ground-
482 based and OMI observations: quality assessment trend analysis and sampling issues.
483 *Atmospheric Chemistry and Physics* **2019**, *19*, 2165–2181.
- 484 (55) Vitt, R.; Laschewski, G.; Bais, A.; Diémoz, H.; Fountoulakis, I.; Siani, A.-M.;
485 Matzarakis, A. UV-Index Climatology for Europe Based on Satellite Data. *Atmosphere*
486 **2020**, *11*, 727.
- 487 (56) Janjai, S.; Wisitsirikun, S.; Buntoung, S.; Pattarapanitchai, S.; Wattan, R.; Masiri, I.;
488 Bhattarai, B. K. Comparison of UV index from Ozone Monitoring Instrument (OMI)
489 with multi-channel filter radiometers at four sites in the tropics: effects of aerosols and
490 clouds. *International Journal of Climatology* **2013**, *34*, 453–461.

- ⁴⁹¹ (57) Laskin, A.; Laskin, J.; Nizkorodov, S. A. Chemistry of Atmospheric Brown Carbon.
⁴⁹² *Chemical Reviews* **2015**, *115*, 4335–4382.
- ⁴⁹³ (58) Gadhavi, H.; Jayaraman, A. Absorbing aerosols: contribution of biomass burning and
⁴⁹⁴ implications for radiative forcing. *Annales Geophysicae* **2010**, *28*, 103–111.
- ⁴⁹⁵ (59) Rios, B.; Raga, G. B. Smoke emissions from agricultural fires in Mexico and Central
⁴⁹⁶ America. *Journal of Applied Remote Sensing* **2019**, *13*, 1.
- ⁴⁹⁷ (60) Barnard, J. C.; Volkamer, R.; Kassianov, E. I. Estimation of the mass absorption cross
⁴⁹⁸ section of the organic carbon component of aerosols in the Mexico City Metropolitan
⁴⁹⁹ Area. *Atmospheric Chemistry and Physics* **2008**, *8*, 6665–6679.

500 Graphical TOC Entry

501



Some journals require a graphical entry for the Table of Contents. This should be laid out “print ready” so that the sizing of the text is correct.

Inside the `tocentry` environment, the font used is Helvetica 8 pt, as required by *Journal of the American Chemical Society*.

The surrounding frame is 9 cm by 3.5 cm, which is the maximum permitted for *Journal of the American Chemical Society* graphical table of content entries. The box will not resize if the content is too big: instead it will overflow the edge of the box.

This box and the associated title will always be printed on a separate page at the end of the document.